4.2 Simulated Lidar Signals for Wake Vortex Detection ahead of the Aircraft

Markus C. Hirschberger[1], Takashi Misaka[1], Frank Holzäpfel[1], Christian Horn[2]
[1]*Institute of Atmospheric Physics,* [2]*Institute of Flight Systems*

Within the DLR-project "Wetter & Fliegen" a feasibility study of airborne lidar sensors for active control at flying through wind shear and turbulent air masses (specifically wake vortices) was carried out. The main goal of such sensors is delivering sufficiently precise real-time measurements of the wind field in a short range in front of an aircraft under clear air conditions up to cruising speed at every altitude, so that a dangerous disturbance in terms of turbulent air motion at an encounter can be alleviated by an active control system with an automatic feed-forward controller. So far, no realized lidar sensor meets the requirements with regard to accuracy, rapidity and spatial resolution of wind measurements necessary for active control. For this reason, we investigate the potential of two suited systems by means of simulations including the physical properties of lidars and atmosphere: a Fringe-Imaging(FI) Doppler Wind Lidar (DWL) similar to the one developed within the project AWIATOR and a Backscatter Lidar (BL) for wind measurements. Though a totally new optical design might be necessary for the latter device to operate at a sufficiently high spatial resolution, the signal processing offers wind components in the *y*- and *z*-directions (transversal to the aircraft's propagation axis *x*) in very short time. From the results of DWL and BL simulations it turns out to be advisable to combine a Fringe-Imaging DWL for the *x*-component measurements with a BL for the *y*- and *z*-component measurements.

Introduction

The superior goal of airline passengers is to arrive on schedule in preferably short time and especially to fly in a safe way at the same time. Although nowadays bigger aircraft are able to transport more passengers per flight, the proliferation of passenger numbers expected in the near future will inescapably raise the number of air activities [3]. In this context, an essential tool for enhancing aircraft throughput while at least preserving the flight safety standards presently in force will be a reliable aircraft-based forward-looking remote sensor or an ensemble of sensors capable of wind measurements at least in a short distance (50-150 m) in front of the airplane, so that a dangerous disturbance in terms of turbulent air motion at an encounter can be compensated by an active control system by means of an automatic feed-forward controller [5,21]. The goal is a lowering of the gust load and an increase in flight comfort by alleviation of incidents with passenger injuries.

Such an active controller application requires precise knowledge of the (turbulent) flow to determine the required counteractions. The forward-looking time should not exceed 0.5 seconds. However, measuring in a shorter time than this is also difficult, due to the lead time necessary for the actuator dynamics and the time needed for the processing of the data measured by the sensor and the subsequent controller positioning computations.

Horizontal or vertical wind shear may cause severe danger for an encountering aircraft, especially near the ground. Turbulence may appear in clouds or in clear air, mainly in the friction layer between about 2000 ft and 3000 ft [23]. The most challenging turbulence phenomenon to cope with are the wake vortices (WV), self-generated by aircraft, that are the major hazard at departure or landing [4]. More flights in the future results in smaller spacings between the separated air corridors, thus the risk of WV encounters increases. Due to their small scale flow structure, wake vortex characteristics are extremely hard to identify by sensors in general. Simple detection of wake vortices is unsatisfactory since their strength varies with age and under the prevailing environmental conditions. Spatial resolution of detection preferably on the order of magnitude of one meter is desirable.

Lidars are remote sensing devices that are capable of wind measurements at high spatial resolution and also in clear air. Here we present two different approaches of useful monostatic pulsed lidars for wind measurements based on simulations. On the one hand a DWL based on the already engineered and flight-tested gust sensor of AWIATOR, that is suitable for measurements even at cruising altitude, will be analyzed numerically, including a critical analysis of the signal processing of the 2D fringes of such a FI-DWL with a FPI, which has not been conducted or published so far for cruise altitude before. On the other hand a more experimental and visionary approach is investigated in detail by simulating a backscatter lidar (BL). The design of this device in combination with its measurement geometry and signal processing is novel.

The objective of this contribution is to show the feasibility of such airborne wind lidar sensors under minimum sensor requirements (for active control).

Measurement Requirements

The general measurement situation is described below in Figure 1 for the DWL case and in Figure 2 for the BL case. Via the radiation backscattered from particles (aerosols or molecules) of the atmosphere, their motion can be captured and this way the wind, which transports them.

While one or multiple lidar(s) situated in the wings of the aircraft should be excluded from analysis (because wings may oscillate strongly and the position of the sensor therefore may vary between the point of radiation emission and detection of the backscattered signal that is analyzed), the aircraft's nose is the only really adequate place for a laser remote sensing device. Thus we restrict our analysis on a monostatic lidar in or near the nose, which also increases the time between measurement in front of the aircraft and actual contact of the wings.

Specifications for a forward-looking sensor for feed-forward control were determined and evaluated based on non-physical sensor models that calculate the measurement points in front of the aircraft. Concerning the necessary data precision of DWL measurements there is a difference between the demands for determination of the disturbance phenomenon from pure LOS-velocities $v_{LOS} = (v_x^2+v_y^2+v_z^2)^{0.5}$ with the respective components [24], and the use of the full 3D wind vector $(u,v,w)^T$ for flight control in the case of a landing approach [10]. Both are compared in Table 1. The requirements for determining the disturbance phenomenon are higher since it does not take three LOS-directions which are necessary to determine one 3D wind vector, but only one LOS-velocity component v_{LOS} each time. Because of the small viewing angles of the LOS-directions in forward-looking lidar configuration, the errors for v_y and v_z (transversal to the propagation direction of the aircraft) are much higher than for v_x.

Table 1: Measurement requirements for (Doppler wind) lidar systems.

Measurement property	disturbance phenomenon (only LOS-velocities)	flight control (full 3D wind vectors)
range	150 m (- 500 m)	30-150 m (120-600 m)
points per slab	min. 63 LOS-directions	min. 20 full 3D wind vectors
frequency (slabs per second)	min. 10 Hz	min. 10 Hz
volume (depth of each slab)	max. 3% of range, i.e. 4.5 m (-15 m)	max. 10% of range, i.e. 3-15 m (12-60 m)
error (standard deviation)	max. 0.5 m/s for v_{LOS}	max. 2.5 m/s for each of u, v, w

For the flight control case knowledge of full 3D wind velocity vectors in front of an aircraft in suitable distances allows the derivation of forces and moments on the aircraft caused by the wind, so that the necessary control commands for compensation can be derived. The measurement error is modelled using normally distributed values with a given standard deviation.

All requirements in Table 1 are valid for landing approach, except the ones in brackets, which are valid at cruising speed (4-5 times higher). In general, the smallest possible value is preferred for the meas-

urement range at flight control depending on the actual air speed. The scan angle depends on the measurement range and should be adapted in order to cover the full wingspan.

Similar parameter values were defined in the project Greenwake [22]. A minimum number of measurement points of 100 for WVs and less than 10 for wind shear is assumed there, with a LOS velocity accuracy of 1 m/s. Operation at all flight levels up to FL400 must be guaranteed.

For the feed-forward controller to work, two kinds of input by measured lidar data are possible:

1. Measured full 3D wind velocity vector (i.e. 3rd column in Table 1). Then the feed-forward controller can directly derive the required control commands.
2. Knowledge of wake vortex circulation, core radius and wake vortex position. Then idealized models like Burnham-Hallock or Lamb-Oseen help derive the necessary wind velocity vectors.

With the first point met with sufficient resolution, the second can also be fulfilled. We aim at measuring the v_x,v_y,v_z components of a single v_{LOS} as good as possible and then take a look at the feasibility of real time processing. Mainly two kinds of lidars have proven their potential to measure wind in the past.

Doppler Wind Lidars (DWL)

While pulsed onboard Doppler radar are capable of long-distance, range-gated wind field measurements under the presence of hydrometeors (e.g. in clouds, fog or rainfall), they are mainly suited for detection of cumulonimbi with high water drop density or for large-scale wind shears only, but not for CAT. Via pulse compression, spatial resolution in the meter-range is possible. Nevertheless, radar will perform poorly under clear air conditions outside clouds, without raindrops or thick optical depths [23]. Compared to Doppler radars, DWL operate well in clear atmosphere. Pulsed DWL measure the wavelength (frequency) shift Δλ, that is caused by the optical Doppler effect, between the emitted laser pulse at the wavelength λ_0 and the received, backscattered photons (including solar photons) at $\lambda_0 \pm \Delta\lambda$ by the LOS-velocity v_{LOS} mentioned above, according to the Doppler shift formula

$$v_{LOS} = -\frac{\Delta\lambda\, c}{2\,\lambda_0}, \tag{1}$$

where $c \approx 3.0 \cdot 10^8$ m/s is the speed of light under the assumption of a refraction index of 1 in clear air. The measurement geometry is displayed in Figure 1.

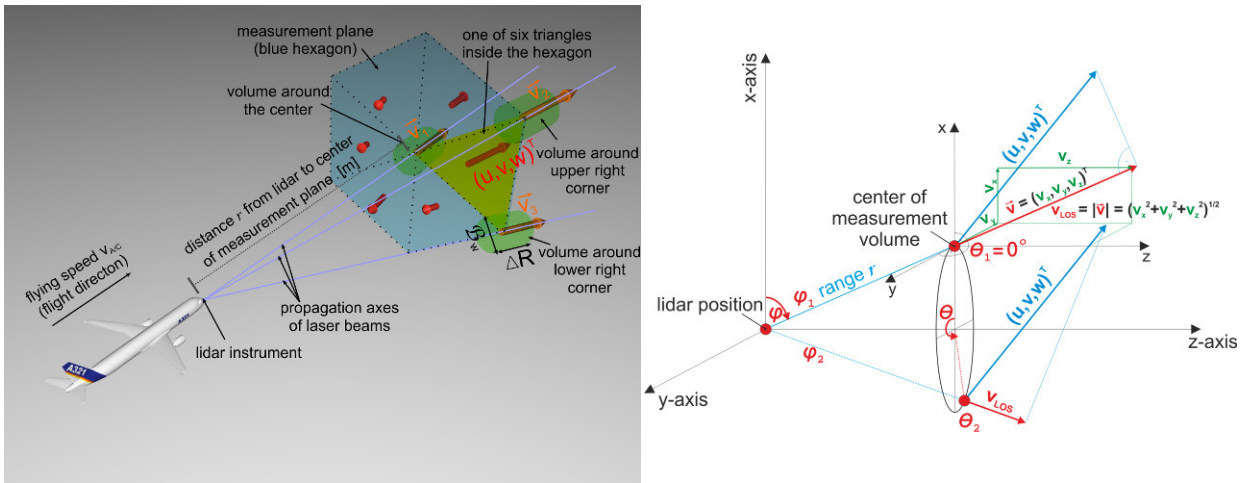

Figure 1. (Left) Measurement geometry with three LOS-vectors $\vec{v}_1, \vec{v}_2, \vec{v}_3$ (orange), i.e. three directions, and full 3D wind vectors $(u,v,w)^T$ (red) generated from three LOS-measurements each (B_W: beam diameter, ΔR: range bin). (Right, taken from [8]) Azimuth and elevation angles with the LOS-velocity components v_x, v_y, v_z of a single LOS-vector $\vec{v}$ (in optical *x*-,*y*-,*z*-coordinates), whose magnitude is v_{LOS}.

Successful aircraft-based measurements of wake vortices with DWL in the past were either near the ground with high aerosol density or in the higher atmosphere only with the help of smoke-seeders or in hazy environment [17]. The angle for the velocity components was very advantageous (huge v_y- and v_z-contributions by measuring the WV from above, and perpendicular to the WV axis, thus the v_y- and v_z-errors are reduced here).

While coherent DWL sensors engineered and tested in projects like MFLAME, I-Wake or FIDELIO were designed for far range measurements (500-2375 m) via heterodyne detection and aerosol backscattering at lower spatial resolution (measurement intervals of ca. 75 m), the incoherent (direct detection via fringe imaging (FI)) FI-DWL sensor of the project AWIATOR was developed for the near field (50-150 m) in front of the aircraft at a slightly higher spatial resolution (ca. 30 m) including the capability of wind detection at cruising altitude by analyzing photons backscattered from molecules [12,19].

The FI-technique of the AWIATOR-sensor allows a combined analysis of the aerosol together with the molecular part of photons in one step, making use of the broadened fringe patterns created by a Fabry-Pérot-interferometer (FPI) on a 2D intensified charge-coupled device (ICCD) localized at the focal plane behind it.

For our needs none of those will be truly satisfactory. Even though big progress has been made concerning the range resolution (ca. 15 m) of heterodyne systems [11] only recently, and with autodyne detection systems being considered [1], all of them are at least today limited in flight altitude because of their need for backscattering aerosols (which are nearly missing completely in cruise altitude) by their measurement principle. The AWIATOR-sensor yields only four LOS-components at a rate of 15 Hz (state 2010), thus nearly no information is gained about a complex structure like a WV. However, this FI-DWL-principle can be extended to more LOS-directions in the future [22].

Backscatter Lidars (BL) for wind measurements

The big advantage of a BL for wind measurements compared to a DWL is its independence of frequency (or wavelength) shifts. This means the Doppler shift needs not be measured and an analyzing interferometer like the FPI is not necessary. The BL works solely with detecting the backscattered intensities (photons) from slabs, i.e. range bins, with a certain thickness in different LOS-directions. The drawback is that two slab measurements at slightly different points of time have to be taken in order to determine the movement of the particles, i.e. the wind velocity. The big advantage is that even under for DWL bad angles (v_y and v_z tiny) and at larger ranges, transversal wind components v and w perpendicular to the flight axis can be measured more quickly and perhaps precise. These transversal wind vector components are crucial to the flight stability of an aircraft. Slab thicknesses for the BL may be smaller than 5 meters and the true air speed needs not be extracted from the results, which is the case for the Doppler shift of DWLs.

The wind evaluation procedure for the v- and w-components of the BL has its origin in Particle Image Velocimetry (PIV) [16]. What is done is a cross-correlation (CC) of two images, taken either from two spatially different slabs d and $d+\Delta d$ at the same point of time t or, more favorable, from the same slab d at two slightly different points of time t and $t+\Delta t$. This laboratory laser principle is applied in the scanning, ground-based Volume-Imaging Lidars (VIL) in the free atmosphere [2,18,20]. The retrieved data are temporarily averaged over volume backscattering measurements, which will not be possible in our airborne case. The flight speed also requires a different scanning device for pulse emission to the directions. Speckle Imaging Velocimetry (SIV) is another lidar method similar to PIV. In SIV the density distribution of the air molecules is measured [6], so far only up to a range of 100 m. Backscattering signals from the slabs include statistically distributed laser-speckle, that serve as indicators for the air motion determined from two CCD image recordings in a small time interval of a small air region. A directional scanner is missing in this device. No tracer particles are added in VIL and SIV measurements.

Figure 2 shows the simulated general principle of an airborne BL for wind measurements proposed in this study. Only a few of the directions of the laser beams are visualized as green lines; in reality or the

simulations the whole measurement plane has to be scanned in a resolution as high as the backscatter images shown. To our best knowledge, so far no fully working airborne BL system for wind measurements has been built or flight-tested. This means, the difficulties arising from a moving platform for the BL system and the signal processing have not been solved yet.

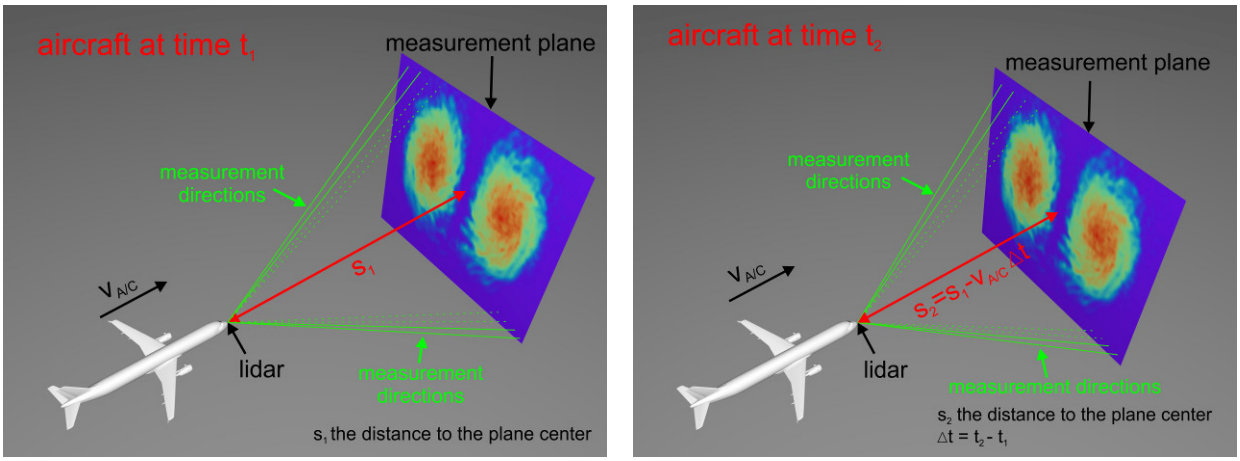

Figure 2. General measurement principle of the simulated airborne BL for wind measurements at times t_1 (left) and $t_2=t_1+\Delta t$ (right). Shown are the backscattered intensity distributions of the simulations. Note that the angles of the measurement directions have to be adapted, i.e. enlarged for the plane at t_2, to scan exactly the same points.

Simulations of a Fringe-Imaging Doppler Wind Lidar

We summarize the results of a paper on simulations of a FI-DWL with a FPI [8]. The interferometric fringe patterns generated by the FPI are simulated including atmospheric conditions as well as laser and detector properties. We focus especially on the noise disturbing the 2D CCD-images in the forward simulation. The backward simulation, i.e. the signal processing, delivers the accuracy achievable via calculation of the ring radii difference of the 2D CCD fringe images between emitted and received photons, and by the Doppler shift formula (1) the LOS-velocity accuracy.

Figure 1 again illustrates the measurement situation for a 3D wind vector geometrically. From three LOS-velocities v_{LOS} in different directions (orange) one full 3D wind vector $(u,v,w)^T$ (red) can be determined (see Figure 1 left, in the centre of the triangle (yellow) formed by the centres of the three LOS-volumes as corners). The question now is: “How exact can a single v_{LOS} be measured?

Because of the quickly changing wind field the measurement plane should be quite close to the aircraft in order to fly through nearly the same wind field as predicted by the DWL (or BL). Thus time for measurement and signal processing is highly limited. The number of backscattered photons would be too low for far-range measurements, since they have to be distributed on a high-resolution CCD (here: 960x780 pixels) for analysis in the FI-DWL-case. The measurement volume is ≈0.05 m^3 for the distances r = 56 (76) m of Table 2 and a range bin of ΔR = 10 m, with assumed values of 0.025 m for the radius of the outgoing laser beam and a divergence angle of 500 µrad at full angle, resulting in a beam width of B_w≈ 0.08 m in the LOS-volume’s center.

Table 2 summarizes the parameters used for the simulations. The backscatter and extinction coefficient values are the ones determined for an altitude of 8500 m. Other properties are the laser wavelength, the instrument constant and the telescope area. The number of backscattered photons received at the CCD is calculated by the single scattering lidar equation. It is n=1.3×10^7 for a LOS-volume range of 76 m and n=2.4×10^7 for a range of 56 m.

Then realistic fringe patterns of a FPI on a 2D CCD localized at the focal plane behind it are simulated, taking atmospheric and instrument properties like scattering and noise into account. The received 13

(24) million photons per pulse are transformed to photoelectrons and distributed on a CCD with 960×780 pixels without intensification. The noisy pixel signals are modeled by Poisson-distributed random numbers for shot (or photon) noise, Gamma-distributed random numbers for speckle noise, and Gauß-distributed random numbers for the read-out noise. Solar background noise plays a minor part due to the short range gates (i.e. low exposure time of Δt = 6.7×10^{-8} s) and can be neglected. Figure 3 (left) shows such a simulated 2D FPI ring pattern on a CCD, that includes strong broadening by Rayleigh scattering. Similar patterns (without atmospheric influences) can also be simulated by 3D ray-tracing of plane waves with random properties, that are emitted towards a FPI (with lenses around it) and finally intersect the 2D CCD-plane. A result is shown in Figure 3 (right).

Table 2. Single scattering lidar equation parameters for a transmitted pulse energy of E_L = 70 mJ and pulse length τ_p = 10 ns at a flight height of h=8500 m used for the FI-DWL simulations.

n	photons received at the CCD	1.3×10^7 / 2.4×10^7
λ_L	center pulse wavelength	354.7 nm
r	range	76 m / 56 m
$\beta(\lambda_L,h)$	backscatter coefficient	3.104×10^{-6} m^{-1} sr^{-1}
A_r	area of the telescope	0.13 m^2
k	instrument constant	0.15
$\alpha(\lambda_L,h)$	extinction coefficient	2.70×10^{-5} m^{-1}
ΔR	range bin of atmospheric volume	10 m

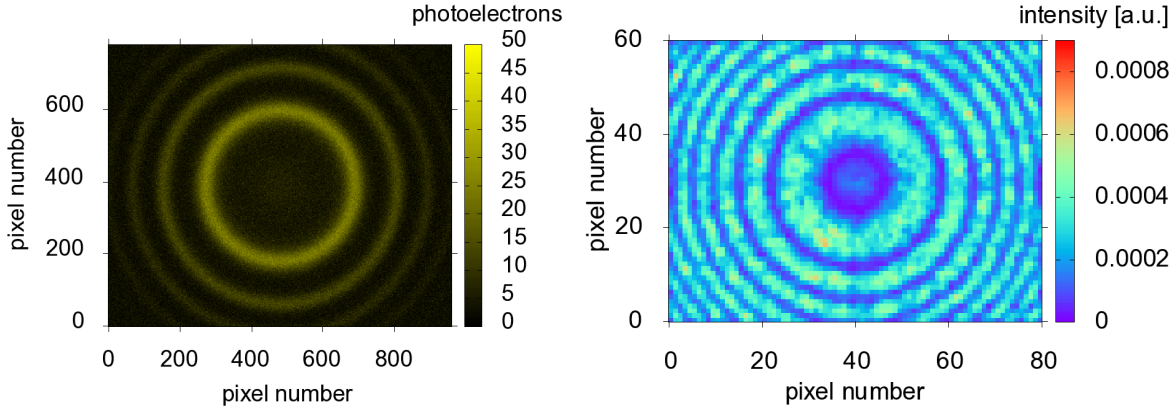

Figure 3. (Left) 2D broadened fringe pattern including atmospheric properties. (Right) 2D fringe pattern on a CCD created via 3D ray-tracing of a multitude of plane waves with random properties.

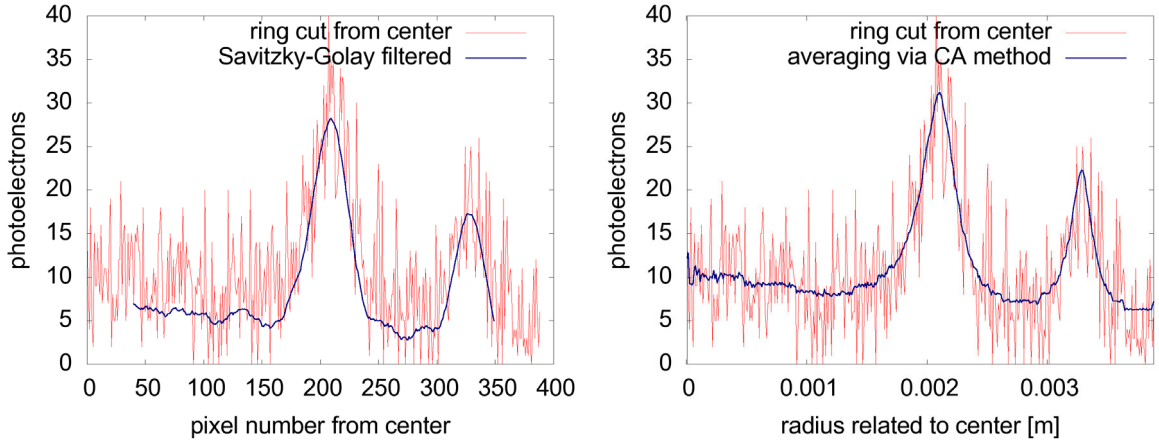

Figure 4. (Left) Cut through a ring from the center to the edge of a 2D-CCD fringe pattern (red) and improvement by Savitzky-Golay-filtering 360 of such noisy cuts in steps of 1° (blue); (Right) Same cut through a ring as in the left image (red), but noise reduction by Circular-Averaging (CA)-method (blue).

The main focus of the signal processing is on two novel radii evaluation strategies including a center determination that make use of the complete 2D information given on the CCD. Thus the noise of single 1D cuts (see red curves in Figure 4) through the 2D rings can be significantly reduced. After calculation of the ring center as exact as possible via the so-called Circular-Averaging(CA)-method, again CA or the so-called Midpoint-Line(ML)-method can be applied to compute ring radii from the CCD-images. CA, when applied to the noisy data, performs better than e.g. a Savitzky-Golay-filter, as visible in the blue curves of Figure 4. In [8], results computed by the ML- and CA-method for a v_{LOS} of 0 m/s and a v_{LOS} of 50 m/s are compared and visualized. The gaps between these curves are tiny; fitting them by the Levenberg-Marquardt method a more precise peak position, which corresponds to the ring radius (i.e. wavelength), is determined.

In the analysis of the results, we have to distinguish the measurement or calculation bias from the standard deviation. The CA-type of signal processing proves to nearly reach the accuracy necessary for LOS-velocity measurements. A standard deviation of 2.5 m⁄s including centre determination can be achieved with only 20 CCD images to average. The bias is 7 m⁄s. For exactly known ring centres, bias and standard deviation can be better than 2 m⁄s for the innermost ring. Especially because of the low number of images (i.e. pulses) necessary to average, the methods are suited for DWL measurements and for use in a velocity sensor on board of aircraft.

However, the precision for the LOS-velocity of more than 0.5 m/s from Table 1 can (if possible) only be reached with even more time-consuming signal processing. Many ways of parallel processing can reduce the computation time. Intensification of a CCD, i.e. an ICCD, may reduce the noise in relation to the received signal, which would result in a higher accuracy. Resolution reduction concerning the pixels to accelerate calculations would yield degraded results.

A FI-DWL may be suitable for short-range wind-shear detection, but not for small-scale phenomena like wake vortices. The Doppler-principle in forward-looking configuration of the lidar favourably measures the v_x-component of v_{LOS} with low error, while results will be more defective for the v_y- and v_z-components due to the small elevation and azimuth angles. Especially these *y*- and *z*-contributions of v_{LOS} are often dangerous for aircraft encountering i.e. a WV. Therefore an alternative approach for the v_y and v_z or the *v*- and *w*-components of a 3D wind vector should be investigated.

Simulations of a Backscatter Lidar for Wind Measurements

A BL has certain advantages in measuring cross-flow velocities compared to a DWL. To simulate such a device we need realistic slabs from complex turbulent structures like wake vortices and a program that takes these profiles as extinctions for backscatter simulations in 3D. The photons backscattered from a slab of wake vortices for the different directions are distributed on a screen as seen by the following aircraft. Finally a cross-correlation procedure and an alternative novel procedure calculate the *v*- and *w*-components of two full backscatter images at slightly different points of time. The software elements necessary to do BL simulations of wake vortices for wind measurements are described now.

Wake Vortex Extinction Profiles from Large Eddy Simulations

For simulation of an airborne BL that measures WVs first of all realistic 3D wind velocity fields generated by WVs are needed. The incompressible Navier-Stokes codes LESTUF and MGLET simulate the circulation decay and vortex topology of WVs as well as the turbulent exchange processes of passive tracers under varying environmental conditions [7,9,13].

For our purpose 3D data from MGLET-simulations of WVs with passive tracers in combination with their velocity field are most suited. (Combined velocity-profiles $(v^2+w^2)^{1/2}$ of LESTUF-simulations also deliver velocity fields similar to Figure 6 left top, that could also be converted to extinction profiles, though these may be physically incorrect structures.)

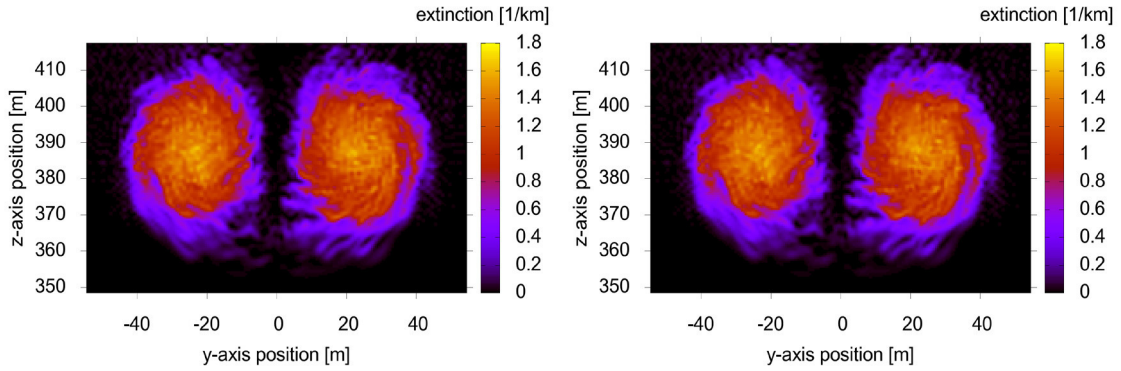

Figure 5. Extinction profiles generated from MGLET simulations at times (left) t_1 and (right) $t_2=t_1+\Delta t$ with Δt=0.1 s for a single slab at high spatial resolution (219×139 pixels). Differences may at least be visible with the naked eye at the dark-yellow centers of the distributions.

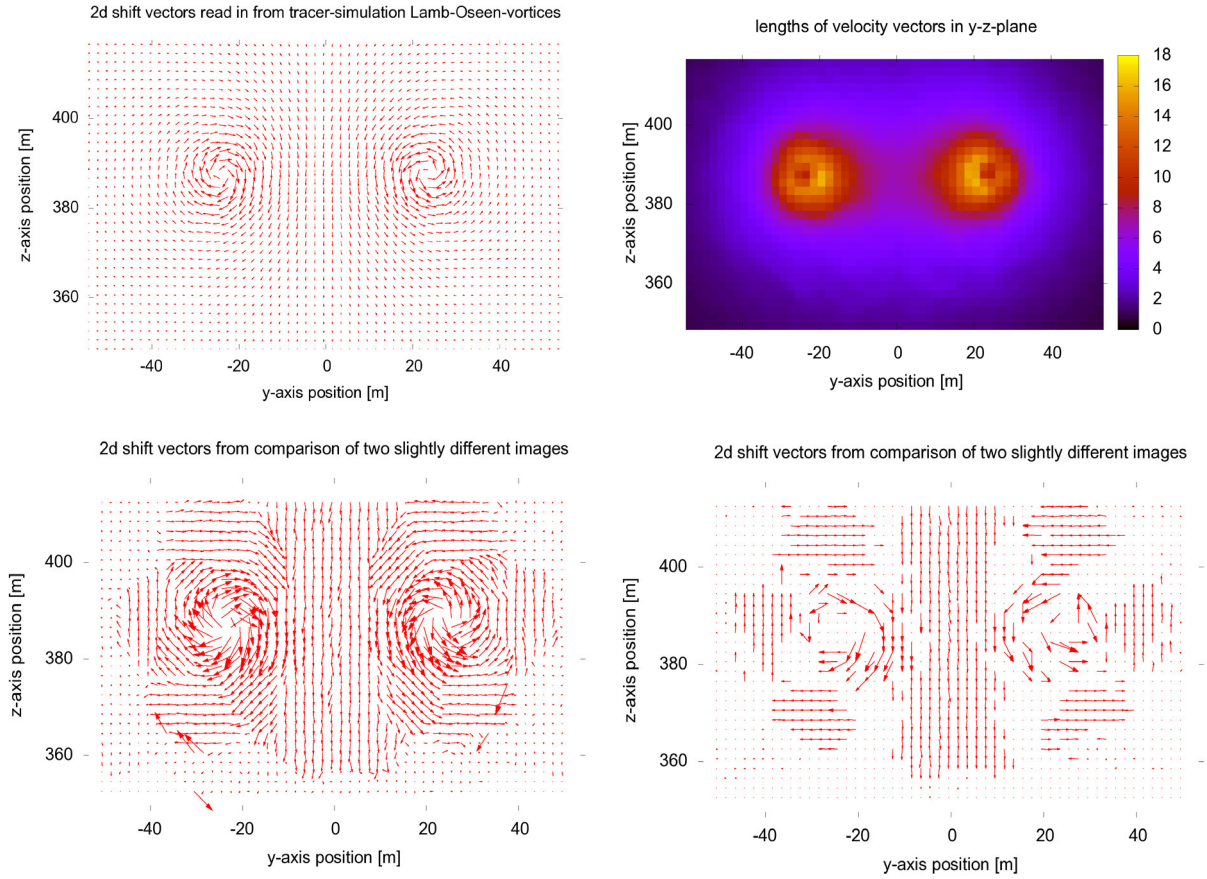

Figure 6. *v*- and *w*-wind velocity components from MGLET-simulations used as an optimal structure (left top), the retrieved wind field from cross-correlation calculations (left bottom) and from weight-shift calculations (right bottom). The lengths (in m/s) of the *v*-and *w*-velocity vector components of the left top image are visualized in the image on the right top.

The resolution of the tracer distributions and the corresponding wind field is usually one meter in all three spatial directions. A case at a vortex age of 40 seconds was chosen, with a normalized eddy dissipation rate (describes the intensity of atmospheric turbulence) of ε*=0.01 and a normalized Brunt-Väisälä-frequency (describes the degree of stable thermal stratification) of N*=0.35, i.e. a still very structured WV without much decay. The WVs generated by a A340 aircraft were modelled in the MGLET simulations as two counter-rotating Lamb-Oseen vortices with a vortex separation of 47.1 meters and a vortex core radius of 3 meters, see Section 6.1.

Since measurements of slabs (planes) should take place at least 10 times per second (see the requirements in Table 1), the movement of the tracers may take only Δt=0.1 s between two images. This is also optimal for the CC-based wind evaluation procedures. However, data from LES-simulations are saved at least every few seconds. Therefore we use 2D velocity fields (*v*- and *w*-component) of slabs perpendicular to the *x*-axis and move the first particle image at time t_1 according to the velocities (e.g. a velocity of 10 m/s means a movement of 1 m in 0.1 s), so that a second particle image at time $t_2=t_1+\Delta t$ is generated. For this short time interval the particle motion should be described physically adequate by this method, and it will serve for a proof-of-principle for the wind-measuring BL later on. Only very close to the vortex centres this method yields artificial radial velocity components (divergence).

As a result from tests with the evaluation algorithms, a higher spatial resolution than 1 m is needed. Therefore the tracer distributions as well as the velocity field from MGLET-simulations taken for the calculation of the second image were spatially interpolated to obtain a resolution of 0.5 meters. This way the images have 219×139 = 30441 pixels and are sufficient to visualize and reconstruct the rotational wind velocity features of the wake vortices in axial view.

Finally, the values of the continuous distributions from MGLET-simulations are raised or lowered to realistic extinction values, while the relative structure of the profile is maintained. Here a stretching factor of 2.0 seems to be suitable. Figure 5 shows the extinction profiles at t_1 and t_2 that are read in for the backscatter simulations. Figure 6 at the left top shows the *v*- and *w*-velocities of a slab at *t*=40 s as given from the MGLET-simulations (optimal) and the same velocity field obtained by the CC-evaluation method (bottom left) and the new Weight-Shift-method (WS) (bottom right) for the extinction profiles to be read in. For better visibility the 2D wind vectors were scaled by a factor of 0.2. Figure 7 shows the differences of the lengths and the directions of the via CC and WS reconstructed velocity vectors from the optimal profile in Figure 6, left top.

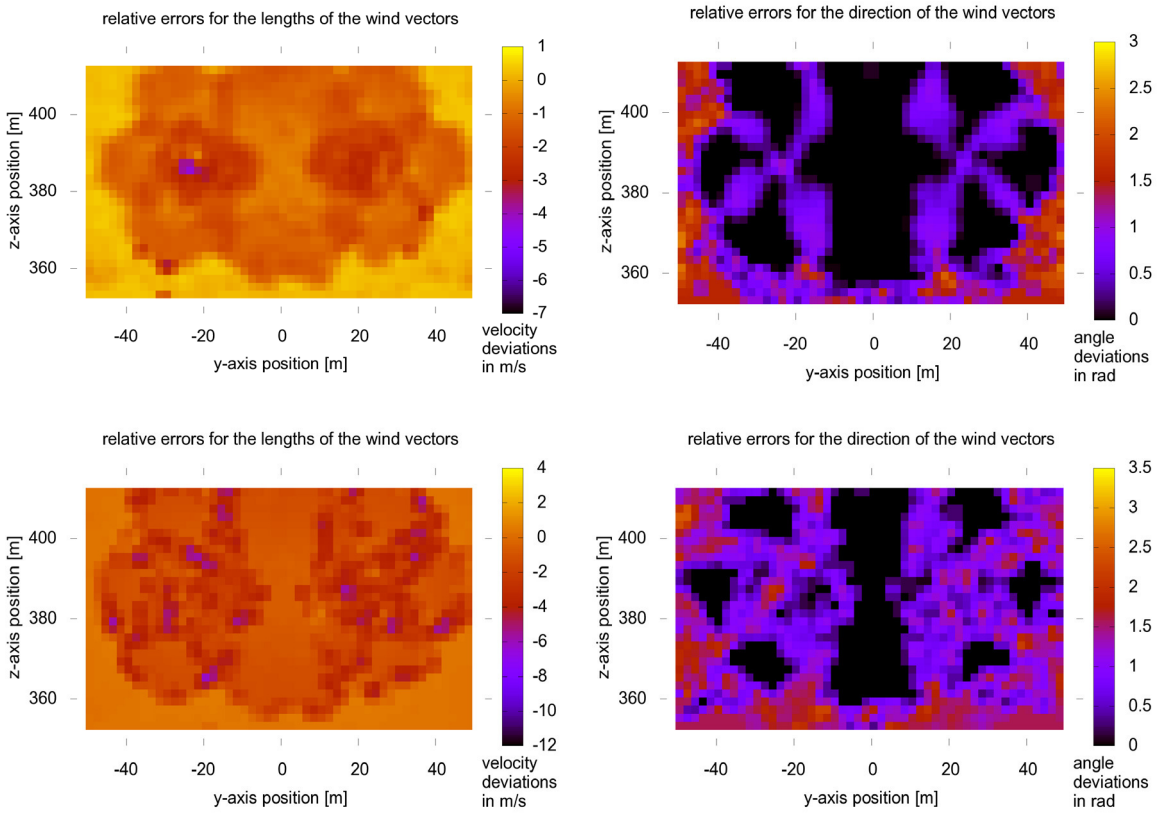

Figure 7. Relative deviations of the velocity magnitudes (in m/s) between the wind field of the large eddy simulation and the wind field calculated from the extinction profiles via CC (top left) and corresponding relative deviations of the wind speed directions (in rad) (top right). The bottom images show the same as the top images for the WS method.

Monte-Carlo Simulations

To perform backscatter simulations we use a Monte Carlo program for polarized backscatter signals (pbs, [14,15]). The contribution of photons hitting a receiver in backward direction is calculated taking polarization into account. The formerly latest version of pbs was adapted concerning its measurement geometry to the necessities of airborne wind-measuring backscatter lidar simulations. The structure of the backscattering volume can be reconstructed more or less exactly if single (weak) pulses are emitted to a multitude of directions with small emitter field of view (equivalent to one beam that is split in multiple directions) rather than emitting a strong single pulse with a large emitter field of view. One reason for this is the lower number of photons in the edge regions of a spatially widened laser pulse.

These problems are eliminated here by a high number of simulated directions (219×139) from a fixed position for the times t_1 and t_2 at 1 million emitted photons per direction. The divergence of each beam, i.e. the emitter field of view is 2 mrad, while the semi-aperture of the receiver is 5 mrad, i.e. the receiver field of view 10 mrad. A Gaussian laser beam is simulated with an input radius of the emitter of maximum 0.1 m, and the radius of the receiver is 0.5 m. Multiple scattering is considered here, although the first scattering order clearly dominates because of the thin slabs and the assumed environmental extinction of 0.1 km^{-1}. The slabs have extinctions up to 1.8 km^{-1}, see Figure 5, and are only 2.5 meters thick.

At the first point of time, t_1, the measurement distance from the lidar to the beginning of the slab we want to measure is 500 m, thus azimuth angles of $-6.2° \le \theta \le 6.2°$ with 219 equidistant subdivisions and elevation angles of $-3.9° \le \varphi \le 3.9°$ with 139 equidistant subdivisions are simulated. At the second point of time, t_2, the distance is only 485 m, i.e. we assume an aircraft flight speed $v_{A/C}$ of 150 m/s in x-direction and an aircraft movement directly to slab, so the aircraft has moved 15 m for the assumed Δt=0.1 s. The maximum angles must be increased: azimuth angles are now $-6.4° \le \theta \le 6.4°$ and elevation angles are $-4.1° \le \varphi \le 4.1°$ at the same resolutions from above. The measurement time intervals are chosen in a way that at θ=0° and φ=0° (beams hitting the center of the slab) just the Δx=2.5 m thick slab is completely measured. This stays the same for the angles outside the center, where the beam will pass a distance slightly longer than 2.5 m. Every part of the slab is (fully) hit by the laser beams.

The scattering Mueller matrices are randomly oriented prolate spheroids at a wavelength of 532 nm (i.e. laser wavelength 532 nm), which have the scattering properties of aerosols. Mueller matrices for molecular scattering could also be used.

The received backscattered photons are then ordered on a screen according to the emission direction of the laser beam, i.e. again 219×139 points. This way the images of Figure 8 are created. Not the absolute photon numbers retrieved are used for analysis, but the backscattering intensities that are normalized according to view angle and measurement distance, so that a comparison by the CC- and WS-algorithms is possible.

A difficulty in reality may be the short time for distinguishing the arriving backscatter contributions from the single directions and slabs (if this is necessary), as well as the adaption of the angle from the first measurement of the plane to the second measurement in a shorter distance in front of a plane. The same plane has to be measured at t_1 and t_2, and this plane has to have exactly the same x-,y- and z-positions and sizes. The particles in it move from t_1 to t_2 according to the extinction profiles.

Calculation of Wind Velocities

The data processing algorithms will be described in detail in the doctoral thesis of M. Hirschberger. The algorithms used here are mainly based on searches for best matches between a chosen reference template of the image 1 at t_1 and a number of equally sized templates in a certain region of the image 2 at t_2.

The cross-correlation (CC)-method first calculates the cross-correlation coefficient functions and searches for a peak value between a reference template of image 1 and all the templates of a certain region of image 2 around this reference template position for these CC-functions. Then the movement of the particles from image 1 to image 2 can be calculated at pixel-accuracy. Finally a Gaussian peak fit

filter is applied to determine the vector shifts at subpixel accuracy [16]. The weight-shift(WS)-method does not use the CC-coefficient functions for best match calculations, but takes the center-of-masses of the templates and computes the best match concerning position of the center-of-mass of a reference template of the image at t_1 and the templates of a region of the image at t_2 around it. Subpixel-accuracy can be reached by filtering with center-of-mass positions. For both methods 8x8 reference templates were used with a search region of 16x16.

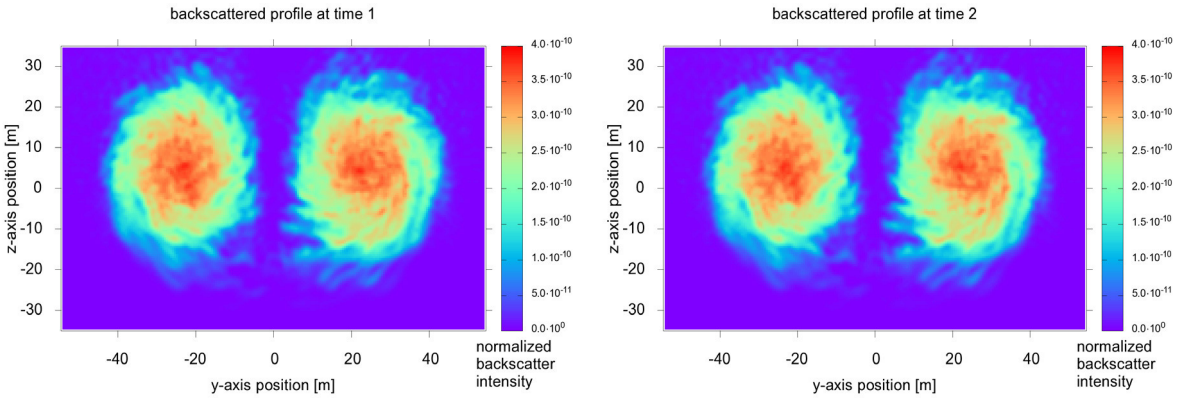

Figure 8. Backscatter images at time t_1 (left) and t_2 (right) from normalized backscatter simulations. The backscattering intensities are normalized according to view angle and measurement distance, so that a comparison by CC- and weight-shift-algorithms is possible.

Results and Discussion

Backscatter Lidar Simulations

Results from the backscatter simulations are presented in Figure 8. Intensities are already normalized, so that the images at t_1 and t_2 can be used for the wind-vector evaluation algorithms. Results of these are shown in Figure 10. Figure 9 visualizes the relative differences of the extinction profiles taken for the simulations (see Figure 5) and the resulting backscatter profiles (see Figure 8). Values are normalized to the averaged values of each image, i.e. each pixel value of both images is divided by this mean value; the difference of these two fractions then yields the differences. Figure 11 finally compares the calculated velocity fields from the extinction profiles (see Figure 6, bottom) with the computed velocity fields from the backscatter profiles (see Figure 10), again for the CC and WS algorithms. See captions of Figures 8 to 11 for more details.

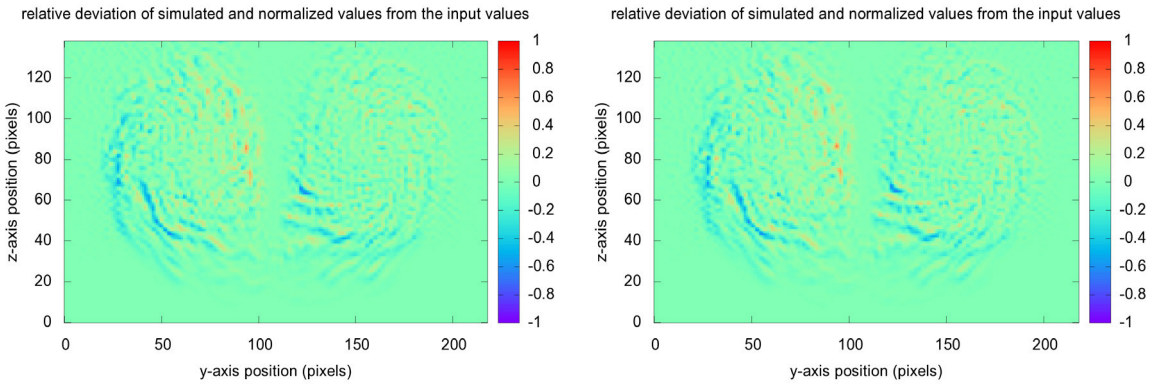

Figure 9. Relative deviations of the average values of read in extinction profile at t_1 and the corresponding backscattered profile at t_1 (left) and the same for the t_2-images (right).

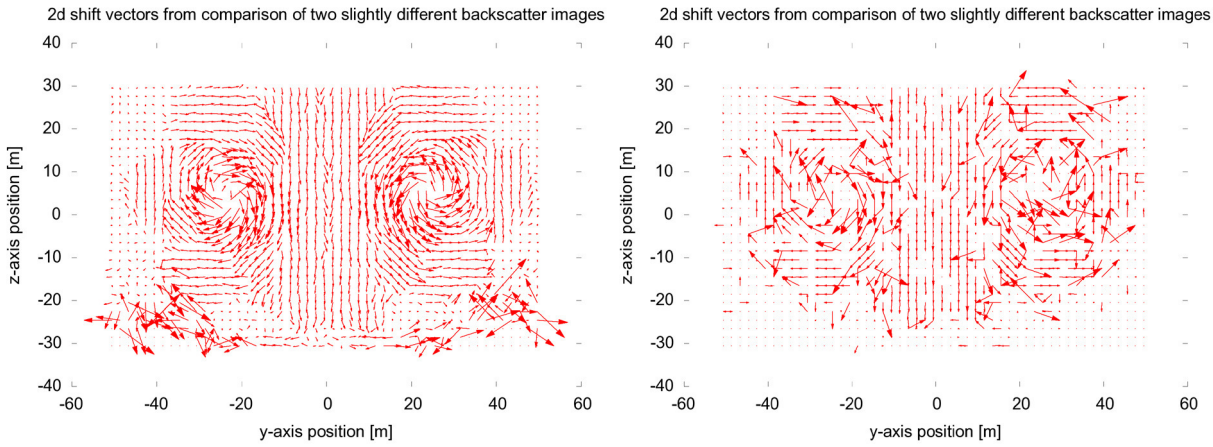

Figure 10. Unfiltered CC-calculated wind vectors (left) and WS-calculated wind vectors (right) in *v*- and *w*-direction from the backscatter images of Figure 8.

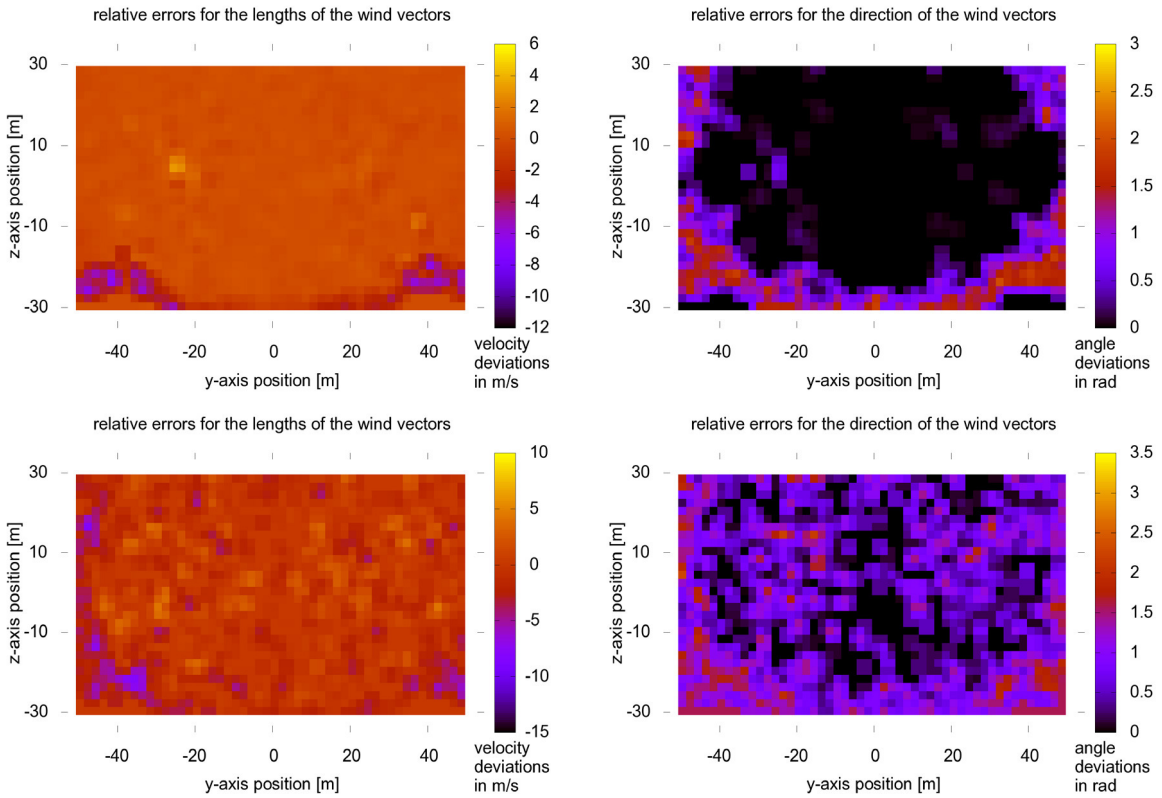

Figure 11. Relative deviations of the velocity magnitudes (in m/s) between the extinction fields and the backscattered fields both calculated via CC (top left) and corresponding relative deviations of the wind speed directions (in rad) (top right). The bottom images show the same as the top images for the WS method.

The results of the simulations of a BL for wind measurements via a proof-of-principle method show the feasibility of detecting the rotational features of vortices, especially with the CC-based algorithm. Errors in the lengths and directions of the retrieved wind vectors are quite low in the center region (see Figures 7 and 11). The number of wind vectors per plane is more than sufficient. However, the *u*-component of wind cannot be simulated so far with backscatter simulations. The main difficulty of this kind of BL in reality is the necessity of many high-resolution slab measurements in very short time gaps, since the CC-algorithms for evaluation are only suited for extremely short time intervals (Δt=0.05-0.2 seconds in

our case; see also PIV) between the two images. The movement of the particles is hardly visible for such small Δt. However, the algorithms can detect them.

The spatial resolution of 219×139 pixels is necessary for detection of the rotational vortex structures and should not be lower to our experience. In PIV laboratory measurements and under useful measurement geometries usually much higher resolutions on ICCD-cameras are measurable. Since time is severely limited for the BL at flight speeds of 70-200 m/s and more, the lidar has not much time to do measurements. A lidar device for measuring in ten-thousands of directions in a few milliseconds seems not to have been built yet. Fibers and beamsplitters could provide a solution for emission of pulses, but in the receiver the backscatter signals may have to be detected according to a time gate for each direction, i.e. the signals from the directions may have to be clearly separated in the detector.

Solar background noise is not relevant at such short time gates (2.5 m slabs) and can be excluded from analysis.

Comparison of Doppler Wind Lidar and Backscatter Lidar

For exactly known FPI ring center at a measurement distance of 56 m and a range bin of 10 m only 20 ring diagrams are sufficient for a bias and a standard deviation better/lower than 2 m/s. (FI-)DWL has big measurement errors for the *v*- and *w*-components of wind. Signal processing is very slow and time-expensive so far. Therefore a BL with new and quick signal processing was analyzed as an alternative. The advantages are visible from the results. The principle of BL would be useful also for wind power stations, where no moving platform must be considered, to measure the wakes behind them or to optimize their orientation to the wind direction. Such a lidar might be much easier to build than for aircraft. Especially the analysis could be extended to 3D, since the lidar could measure more than just a few slabs (see also [20]).

Conclusion and Outlook

So far, no suitable lidar sensor for active flight control is available. From the results of DWL and BL simulations it turns out to be advisable to combine a FI-DWL for the *x*-velocity component measurements with a BL for the *y*- and *z*-velocity component measurements. Possibly, the vortex velocities in flight direction are less important for active flight control such that crossflow measurements with a BL would be sufficient.

Concerning the BL as a wind-measuring device, the simulations should also be possible for a measurement distance lower than 500 meters, although this may be difficult in the simulations (not in reality) because of the wider angles of view; slabs thinner than 2.5 m could alleviate this problem. Photon noise should be included in the analysis, and laser wavelengths different from 532 nm should be simulated, since lasers at 532 nm might not be eye-safe. There is still a lot of potential in the analysis algorithms for the BL. The analysis for BL could for example be extended to the 3D case, so a full 3D wind vector would become available. At *y*- and *z*-resolutions of 0.5 m this means slabs of only Δx=0.5 m thickness and a high number of such thin slabs to be measured. Simulations could become too time-consuming for realization in that case.

Acknowledgements

We would like to thank G. Ehret, N. Hannemann, I. Hennemann, M. Moser, O. Reitebuch, F. Steinebach and C. Wolkensinger. A special thanks to U.G. Oppel and to M. Wengenmayer for the former latest version of pbs, as well as to T. Gerz and C. Schwarz for managing the project.

References

[1] M.C. Cates, J.N. Paranto, T.A. Larsen (2011), Multifunction Aircraft Light Detection And Ranging (LIDAR), Patent-No. WO/2011/022164 A1.

[2] E.W. Eloranta, J. King, J.M. Weinman (1975), The determination of wind speeds in the boundary layer by monostatic lidar, J. Appl. Meteorol. 14, 1485-1489.

[3] EUROCONTROL (2004), Challenges to Growth 2004 Report (CTG04), European Organization for the Safety of Air Navigation, Edition Number 1.0, EATMP Infocentre Reference 041109-01, Brussels, Dec. 2010.

[4] T. Gerz, F. Holzäpfel, D. Darracq (2002), Commercial aircraft wake vortices, Progress in Aerospace Sciences 38, 181-208.

[5] K.-U. Hahn, D. Fischenberg, D. Niedermeier, C. Horn (2010), Wake Encounter Flight Assistance Based on Forward-Looking Measurement Processing, In: AIAA Guidance, Navigation, and Control Conference, 2-5 August 2010, Toronto, Ontario Canada, AIAA 2010-7680.

[6] T. Halldórsson, A. Langmeier, A. Prücklmeier, V.A. Banakh, A. Falits (2006), Particle and speckle imaging velocimetry applied to a monostatic lidar, Proc. SPIE 6522, 65220A.

[7] I. Hennemann, F. Holzäpfel (2011), Large-eddy simulation of aircraft wake vortex deformation and topology, Proc. IMechE Vol. 225 Part G: J. Aerospace Engineering, published online 23. September 2011, DOI: 10.1177/0954410011402257.

[8] M.C. Hirschberger, G. Ehret (2011), Simulation and high-precision wavelength determination of noisy 2D Fabry-Pérot interferometric rings for direct-detection Doppler lidar and laser spectroscopy, Appl. Phys. B 103, 207-222, link: http://www.springerlink.com/content/u3311lvg67060665/ .

[9] F. Holzäpfel, T. Misaka, I. Hennemann (2010), Wake-Vortex Topology, Circulation, and Turbulent Exchange Processes. In: AIAA Atmospheric and Space Environments Conference, 2-5 August 2010, Toronto, Ontario, Canada, AIAA 2010-7992.

[10] C. Horn, C. Schwarz (2009), Sensor Requirements for a feed forward controller, internal report of the DLR project “Wetter und Fliegen”, June 2009.

[11] H. Inokuchi, H. Tanaka, T. Ando (2009), Development of an Onboard Doppler Lidar for Flight Safety, J. Aircraft 46, 1411-1415.

[12] G. Jenaro Rabadan, N.P. Schmitt, T. Pistner, W. Rehm (2010), Airborne Lidar for Automatic Feedforward Control of Turbulent In-Flight Phenomena, J. Aircraft 47, 392-403.

[13] T. Misaka, F. Holzäpfel, T. Gerz, M. Manhart, F. Schwertfirm (2011), Large-Eddy Simulation of Wake Vortex Evolution from Roll-Up to Vortex Decay, In: 49th AIAA Aerospace Sciences Meeting including the New Horizons Forum and Aerospace Exposition, 4-7 January 2011, Orlando, Florida, USA, AIAA 2011-1003.

[14] U.G. Oppel, M. Wengenmayer (2003), Diffusion of the lidar beam seen from the receiver. In: C. Werner, U.G. Oppel, T. Rother: 12th International Workshop on Lidar Multiple Scattering Experiments (MUSCLE XII), 10-12 Sept. 2002, Oberpfaffenhofen, Germany, Proc. SPIE 5059, pp. 21-30.

[15] U.G. Oppel, M. Hirschberger, M. Wengenmayer (2006), Simulation of the azimuthal dependence of cross-polarized lidar returns and its relation to optical depth and a comparison with measurements by N. Roy, G. Roy, L.R. Bissonnette, and J.-R. Simard. 14th International Workshop On Multiple Scattering Lidar Experiments (MUSCLE XIV), Université Laval, Québec, Canada, 4-7 Oct. 2005, pp. 27-40. Defence R&D Canada, Valcartier.

[16] M. Raffel, C. Willert, S. Wereley, J. Kompenhans (2007), Particle Image Velocimetry - A Practical Guide (2nd ed.), Springer-Verlag Berlin Heidelberg.

[17] S. Rahm, I. Smalikho, F. Köpp (2007), Characterization of Aircraft Wake Vortices by Airborne Coherent Doppler Lidar, J. Aircraft 44, 799-805.

[18] Y. Sasano, H. Hirohara, T. Yamasaki, H. Shimizu, N. Takeuchi, T. Kawamura (1982), Horizontal wind vector determination from the displacement of aerosol distribution patterns observed by a scanning lidar, J. Appl. Meteorol. 21, 1516-1523.

[19] N.P. Schmitt, W. Rehm, T. Pistner, P. Zeller, H. Diehl, P. Navé (2007), The AWIATOR airborne LIDAR turbulence sensor, Aerosp. Sci. Technol. 11, 546-552.

[20] J.L. Schols, E.W. Eloranta (1992), Calculation of Area-Averaged Vertical Profiles of the Horizontal Wind Velocity From Volume-Imaging Lidar Data, J. Geophys. Res. 97, 18395-18407.

[21] C. Schwarz, K.-U. Hahn (2011), Automated pilot assistance for wake vortex encounters, Aerosp. Sci. Technol. 15, 416-421.

[22] C. Schwarz, S. Bowater (2011), UV Imaging Lidar for Wake Vortex Detection - The GreenWake Project, Project Progress Review, May 2011, link: http://www.wakenet.eu/fileadmin/user_upload/3rd%20Major%20Workshop/presentations/WN3E_3rdMW_day2_Greenwake.pdf (Nov. 2011).

[23] C. Wolkensinger (2010), Vergleich messtechnischer Konzepte zur bordgestützten Ermittlung atmosphärischer Störphänomene, DLR Institut für Flugsystemtechnik, Braunschweig, IB 111-2010/35, 59 pages.

[24] C. Wolkensinger (2011), Autonomous Wake-Vortex Approximator (AWA): Autonomes Verfahren zur Erkennung von Wirbelschleppen aus Line-of-Sight (LoS) Messdaten eines vorausschauenden Sensors, DLR Institut für Flugsystemtechnik, Braunschweig, IB 111-2011/14, 35 pages.